Biosensors and Bioelectronics 25 (2009) 147–153

Contents lists available at ScienceDirect

Biosensors and Bioelectronics

journal homepage: www.elsevier.com/locate/bios

# Intervention of cardiomyocyte death based on real-time monitoring of cell adhesion through impedance sensing

Yiling Qiu [a], Ronglih Liao [b], Xin Zhang [a,*]

[a] Laboratory for Microsystems Technology, Department of Mechanical Engineering, Boston University, Boston, MA 02215, United States
[b] Brigham and Women's Hospital, Harvard Medical School, Boston, MA 02115, United States

ARTICLE INFO

*Article history:*
Received 30 April 2009
Received in revised form 11 June 2009
Accepted 16 June 2009
Available online 24 June 2009

*Keywords:*
Cell death
Cardiomyocyte
Tumor necrosis factor α
Impedance sensing

ABSTRACT

Cardiomyocyte death caused by proinflammatory cytokines, such as Tumor necrosis factor α (TNF-α), is one of the hot topics in cardiovascular research. TNF-α can induce multiple cell processes that are dependent on the treatment time although the long-term treatment definitely leads to cell death. The ability to intervene in cell death will be invaluable to reveal the effects of short-term TNF-α treatment to cardiomyocytes. However, a real-time monitoring technique is needed to guide the intervention of cell responses. In this work, we employed the impedance-sensing technique to real-time monitor the equivalent cell–substrate distance of cardiomyocytes via electrochemical impedance spectroscopy (EIS) and electrical cell–substrate impedance sensing (ECIS). In the stabilized cardiomyocyte culture, the sustained TNF-α treatment caused strengthened cell adhesion in the first 2 h which was followed by the transition to cell detachment afterwards. Considering cell detachment was an early morphological evidence of cell death, we removed TNF-α from the cardiomyocyte culture before the transition to achieve the intervention of cell responses. The result of this intervention showed that cell adhesion was continuously strengthened before and after the removal of TNF-α, indicating the short-term treated cardiomyocytes did not undergo death processes. It was also demonstrated in TUNEL and TBE tests that the percentages of apoptosis and cell death were both lowered.



## 1. Introduction

Cardiomyocyte death caused by proinflammatory kinases, such as Tumor necrosis factor α (TNF-α), has been implicated as a fundamental patho-physiological mechanism in a variety of heart diseases, such as acute myocardial infraction, congestive heart failure or congenital heart diseases (Cook and Poole-Wilson, 1999; Haunstetter and Izumo, 1998). There are multiple death pathways that can be triggered by the proinflammatory kinases. When TNF-α, a proapoptotic stimuli, binds with tumor necrosis factor receptor I (TNFR-I), a death receptor, it will provokes caspases to execute the apoptosis process (Hengartner, 2000). High concentration level of TNF-α can even induce necrotic cell death due to its toxicity (Qiu et al., 2009). However, various pathways of cell death are not the only outcomes of TNF-α treatment. TNF-α also triggers hypertrophy simultaneously, though the sustained long-term overexpression of TNF-α eventually leads to apoptosis (Packer, 1995). In the death processes of cardiomyocytes, no matter apoptosis or necrosis, cell adhesion will be weakened. In the signaling pathways of apoptosis induced by TNF-α or other proinflammatory kinases, caspases, the central executioners of apoptosis (Hengartner, 2000), mediate a series of cleavage of essential proteins, including focal adhesion kinase (FAK), at the early phase of the apoptosis. The inactivation of FAK causes immediate cell detachment from adjacent cells or ECM. On the other hand, in the necrosis process, the rapture of cell membrane also causes cell detachment from its neighborhood. If the ongoing cell detachment of cardiomyocytes can be detected, it is possible to prevent cardiomyocytes from cell death by intervening in the cell responses to stimuli before the exclusive death process. The ability of intervention suggested the possibility of obtaining the transient or unstable behavior of cells, and thus will be significantly beneficial to the pathological or pharmacological research of proinflammatory kinases. Nevertheless, current techniques are not sensitive enough to provide real-time monitoring of such subtle cell responses noninvasively and quantitatively, and thus there is no detailed information to guide the intervention of cell responses.

Electric cell–substrate impedance sensing (ECIS), first defined by Giaever, is a noninvasive and sensitive detection technique for cell adhesion (Giaever and Keese, 1984, 1993), in which the impedance time course of cell-covered electrodes is recorded and attributed to various cell behaviors. In the last two decades, ECIS sensing has been employed to monitor many types of cells, including fibrob-

* Corresponding author at: The Photonics Center, Rm. 936, Boston University, 8 Saint Mary's Street Boston, MA 02215, United States. Tel.: +1 617 358 2702; fax: +1 617 353 5548.
*E-mail address:* xinz@bu.edu (X. Zhang).

0956-5663/$ – see front matter © 2009 Elsevier B.V. All rights reserved.
doi:10.1016/j.bios.2009.06.027

lasts, endothelial cells, cancer cells, etc. (Earley and Plopper, 2006; Kowolenko et al., 1990; Luong et al., 2001; Tiruppathi et al., 1992; Xiao et al., 2002). More recently, ECIS research turned to excitable cells, such as skeletal muscle cells (Aas et al., 2002) and cardiomyocytes (Yang et al., 2007; Yang and Zhang, 2007). To extract direct and detailed information from the overall signals, researchers (Giaever and Keese, 1991; Lo and Ferrier, 1998) further developed advanced data processing techniques. In these methods, morphological parameters, such as cell–substrate distance, are solved for precise description of cell adhesion (Giaever and Keese, 1991; Lo et al., 1995). It has been reported that the ECIS method is capable of detecting vertical motion in the order of 1 nm (Giaever and Keese, 1993). Combining with other biophysical and biochemical assays, ECIS had been applied to study apoptosis of endothelial cells (Arndt et al., 2004). However, unlike endothelial cells or fibroblasts in the reported ECIS cases which exhibit known and constant electrical properties due to the reliable commercialized cell lines, cardiomyocytes are primarily cultured, which means unknown and unstable electrical properties have to be solved for each sample. In our preliminary research (Qiu et al., 2008, 2009), a real-time monitoring technique has been developed on the basis of electrochemical impedance sensing (EIS) and electrical cell–substrate impedance sensing (ECIS). In this technique, equivalent cell–substrate distance is used to describe the extent of cell adhesion.

In this work, our impedance-sensing technique was employed to real-time monitor the cardiomyocyte culture. The response of cardiomyocytes to TNF-α was recorded in time courses of equivalent cell–substrate distance. The transition from cell adhesion to detachment was detected in the continuous treatment of TNF-α. TNF-α was removed from the cardiomyocyte culture as the intervention of cell responses before the critical moment of transition, which resulted in continuously enhancement of cell adhesion and prompted cell viability. Biochemical tests, such as TUNEL and TBE, were employed to examine the apoptosis percentage and death percentage of cardiomyocytes. Our results demonstrated how our real-time impedance-sensing technique could be used to guide the intervention of cell responses, which could lead to further development of cell-regulation techniques based on impedance sensing.

## 2. Materials and methods

### 2.1. Fabrication

The fabrication of the impedance-sensing chips was conducted in a microfabrication laboratory. A glass slide was chosen as the substrate material because it could minimize the substrate capacitance and decrease the measurement noise. The electrode voids of the chips were patterned on the slides with photoresist Shipley 1813 in photolithography on the MA6 aligner. Effective adhesion of the metal electrodes to the glass substrate was required, therefore a chromium layer (125 Å) was first deposited in thermal evaporation, followed by the deposition of the major electrode components with gold (375 Å) (Kurt J. Lesker Co.). The metal electrodes were defined in a lift-off process. $SiO_2$ and $SiN_x$ (Kurt J. Lesker Co.) were deposited with magnetic sputtering to form an insulating layer with a thickness of 1200 Å. Windows were defined in the insulating layer using photolithography and opened by reactive ion etching to access the gold electrode surface. A biosensing chip consisted of 16 circular working electrodes (0.502 $mm^2$) and one common rectangular counter electrode (2.0 $cm^2$). Fig. 1a shows the configuration of the biosensing chip.

### 2.2. Testing systems

The schematic diagram and photo of our impedance-sensing system is depicted in Fig. 1b. The biosensing chip was maintained

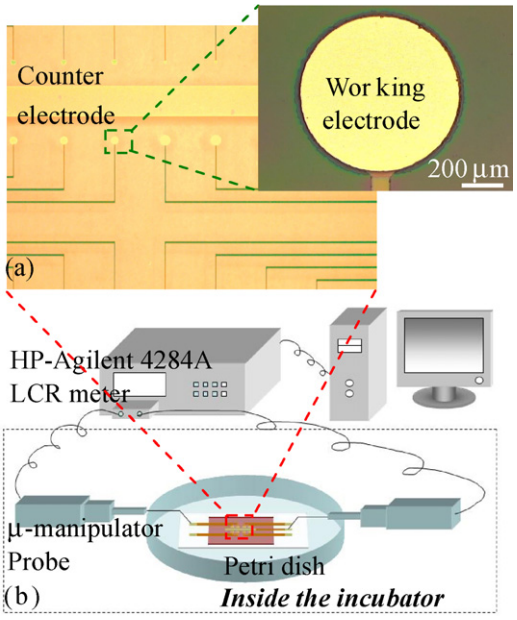


**Fig. 1.** (a) Top view and close view of the counter and working electrodes fabricated in a lift-off process (Cr/Au: 125 Å/375 Å). Chromium was used to increase the adhesion of the gold layer to the glass substrate. A laminin (an ECM protein) layer was coated before cardiomyocytes were injected. (b) Schematic diagram of the impedance measurement system. The part surrounded by dash lines was inside the incubator (37 °C, 5% $CO_2$).

in the incubator at 5% $CO_2$ and 37 °C throughout the electrical measurement to avoid any fluctuations in the testing environment. Inside the incubator, the biosensing chip was mounted to a homemade silicone chamber designed for cell culture. The electrode pads were connected to micromanipulators, which transferred signals through an Agilent 16048A BNC test fixture to the outside of the chamber. The impedance of the electrodes in the chip was measured with an Agilent 4284A LCR meter (Agilent Technologies Inc., CA). For automatic measurement and data logging, the LCR meter was connected to a computer through a GPIB interface. The impedance measurement process was controlled by LabView (National Instruments Corp., Austin, TX) virtual instruments.

### 2.3. Cardiomyocyte isolation and culture

Left ventricular (LV) myocytes were isolated from male Wistar rats according to a previously established protocol with some modifications (Lim et al., 2001). The rat heart was separated and perfused with $Ca^{2+}$-free Krebs buffer (0.12 mol/L NaCl, 4.7 mmol/L KCl, 1.2 mmol/L $KH_2PO_4$, 1.2 mmol/L $MgSO_4$, 25 mol/L $NaHCO_3$, and 12 mmol/L glucose) and enzyme buffer (375 mg/L Collogenase and 425 mg/L Hyaluronidase in $Ca^{2+}$-free Krebs buffer). The rat heart was then cut into 8 to 10 small pieces and dispersed in enzyme buffer (Trysin 0.3 mg/mL and DNAase 0.3 mg/mL in $Ca^{2+}$-free Krebs buffer). The cardiomyocyte suspension was subsequently filtered through a nylon mesh, resulting in a typical yield of >90% rod-shaped cells. The isolated cells were then washed with DMEM, and were ready for plating onto microelectrodes. For the ECM, a laminin suspension was prepared by diluting the laminin solution (Becton-Dickinson) in serum-free medium at volume ratio of 1:100. The laminin suspension was dropped onto the impedance-sensing electrodes which were then kept still in the incubator for at least 30 min until a laminin layer formed. For electrical measurement, the biosensing chip was inoculated with 1.5 mL of the cardiomyocyte suspension for a population density of $5 \times 10^4/cm^2$.

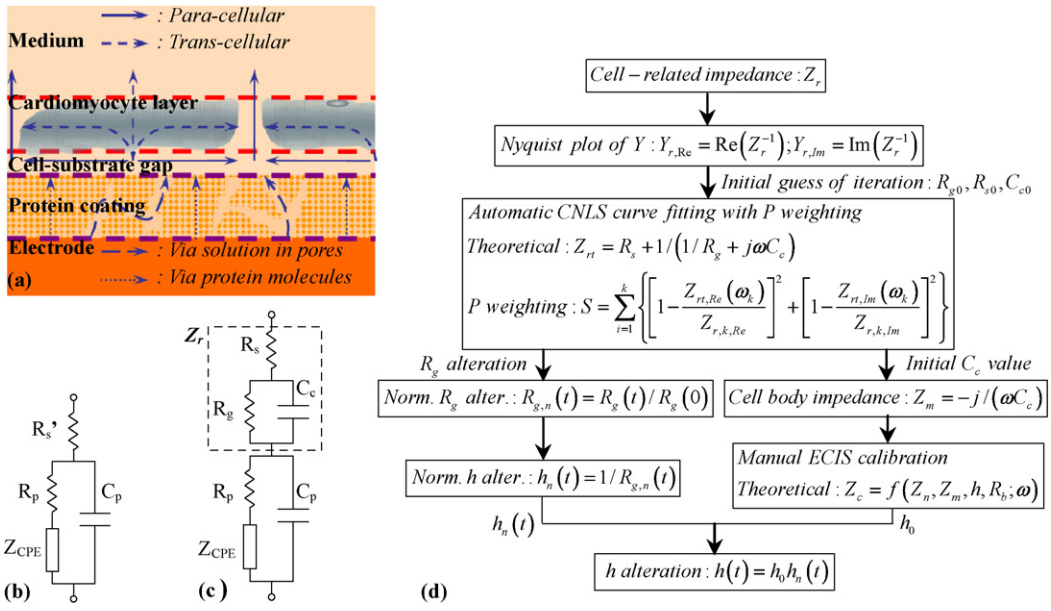


**Fig. 2.** (a) Current flow patterns on the testing electrode. There are two modes of current in protein coating layer: one travels via solution in the pores among protein molecules; the other travels via protein molecules. There are also two modes of current in cardiomyocyte layer: Para-cellular mode represents how the current travels in solution around cells; trans-cellular mode represents how the current travels through the cell body. (b) Equivalent circuit model of impedance of the cell-free system ($Z_n$). (c) Equivalent circuit model of impedance of the cell-covered electrode ($Z_c$). (d) The data processing procedure for calculating the equivalent cell–substrate distance of cardiomyocytes.

### 2.4. Impedance spectra

The measurement of impedance was performed with 80 frequencies logarithmically evenly spaced between 20 and 200 kHz, with a 5-mV voltage excitation. One round of frequency scanning was completed in 1 min. For the continuous monitoring, the cyclic frequency scanning was applied to the testing system every 10 min. The impedance data were recorded as real and imaginary components accompanied by the testing frequency in a txt file, which was convenient for the following data processing and analysis. The specific impedance values were calculated by multiplying the measured values by the area of working electrode. In the following description, the electrical parameters, including impedance, admittance, resistance and capacitance were all recorded as specific values.

### 2.5. Models and data processing

The equivalent circuit model of cell-free system was shown in Fig. 2b where capacitor $C_p$ and resistor $R_p$ were used to represent the capacitance and resistance of the porous laminin layer (schematic in Fig. 2a). A constant phase element (CPE) was used to account for the nonlinearities of frequency-related electrical double layer impedance on the uncovered electrode surface ($Z_{CPE} = [Q_{CPE}(j\omega)^n]^{-1}$, where $j$ and $\omega$ were the imaginary unit and angular frequency respectively) (Bard and Faulkner, 2003; Tlili et al., 2003). Resistor $R_s'$ was the solution resistance. This model was fit and modified to the 3D impedance response plot in a complex nonlinear least square (CNLS) curve fitting program. The $P$ weighting (Barsoukov and Macdonald, 2005) was added into the objective function of CNLS curve fitting to ensure the validity in case the fitting to the real and imaginary component of cell-free impedance ($Z_n$) was unbalanced. Despite the existing curve fitting software, for example, LEVM, a CNLS curve fitting program was written based on the optimizing toolbox of MATLAB. This allowed for a convenient means the impedance data obtained in LabView virtual instruments and the following calculations and plotting.

The cell-related impedance ($Z_r$) was represented with three elements in the equivalent circuit model of cell-covered system (Fig. 2c). $C_c$ was used to represent the reactance of cells and $R_g$ was used to describe the resistance of the thin medium layer in the cell–substrate gap. $R_s$ was the resistance of bulk medium body. To achieve in the automation in determining the element parameters, the cell-related admittance response ($Y_r = Z_r^{-1}$) was first analyzed in a Nyquist plot. The electrical parameters acquired in the Nyquist plots of $Y_r$ were utilized as the iterative initial of the following CNLS curve fitting. Every loop in the cyclic frequency scanning went through the EIS data processing to determine $R_g$, $R_s$ and $C_c$ values.

In our methodology, the time course of equivalent cell–substrate distance ($h$) was obtained via the data processing procedure illustrated in Fig. 2d (Qiu et al., 2008). Since $R_g$, the ion-conductive resistance, obeyed the Ohm's law, it would be reasonable to define the normalized equivalent cell–substrate distance ($h_n$) was inversely proportional to the normalized $R_g$. Since we were able to collect the time course of $R_g$ through the EIS data processing, the time course of $h_n$ could also be obtained. The absolute cell–substrate distance was calculated with Lo's ECIS model of cell (Lo and Ferrier, 1998) in which expression was given out for the relation between impedance values and the morphological values, such as absolute cell–substrate distance. Among these values, the impedances of cell-free ($Z_n$) and cell-covered system ($Z_c$) could be measured, while the cell membrane impedance was considered as capacitive reactance ($Z_m = -j/(\omega C_c)$). Once the absolute cell–substrate distance at the initial moment ($h_0$) was obtained through Lo's ECIS model with the manually selected iterative initial, the real time recording of equivalent cell–substrate distance could be achieved by multiplying the time course of $h_n$ with $h_0$. This method was also employed in the following experiments.

### 2.6. TNF-α-treatment, TBE tests and TUNEL tests

TNF-α (Sigma–Aldrich Co.) treatment was carried out in serum-free media after 24-h culture for stabilizing. TNF-α was applied to the cultured cardiomyocytes at the concentration level of 10 ng/mL. The cyclic frequency scanning was applied to samples as soon as the TNF-α treatment began.

TBE test was conducted with 0.4% Trypan blue solution (Sigma–Aldrich). The applied concentration of Trypan blue was

5% (v/v). The samples were analyzed on a fluorescent microscope (Nikon Eclipse TS100-F).

TUNEL test was performed with the In Situ Cell Death Detection Kit, Fluorescein (Roche Applied Science Co.). After the treatment with TNF-α, cardiomyocytes were washed three times in phosphate buffered saline (PBS) and then fixed with 4% paraformaldehyde in PBS for 1 h at room temperature. Cardiomyocytes were then permeabilized for 2 min on ice with 0.1% Triton X-100 in 0.1% sodium citrate. After rinsing the sample twice with PBS, 50 μL TUNEL reaction mixtures were added on the cardiomyocytes, followed by incubation for 1 h in a humidified and dark chamber. Cardiomyocytes were rinsed three times with PBS and strained with DAPI (4′,6-diamidino-2-phenylindole).

## 3. Results and discussion

### 3.1. Characterization of impedance-sensing system

Since cardiomyocytes could only be cultured on ECM proteins, a laminin layer was deposited onto the working electrodes before injecting in the cells and kept quiescence for at least 30 min. Then the cell-free working electrode was characterized through fitting the measured impedance spectra to the equivalent circuit model. The element parameters were determined in the CNLS curve fitting (Fig. 3a) for the cell-free impedance-sensing system: $R'_s = 2.21 \pm 0.07\ \Omega\,cm^2$, $C_p = 5.59 \pm 0.24\ \mu F/cm^2$, $R_p = 2.30 \pm 0.19\ \Omega\,cm^2$, $Q_{CPE} = 125.03 \pm 0.51\ \mu F/cm^2$, $n = 0.806 \pm 0.004$.

In order to evaluate the influence of TNF-α to the resistance of solution, a comparison was made to solutions with multiple concentrations of TNF-α. The examined TNF-α concentrations were all within the physiological range. There was no obvious difference between the solution resistances ($R'_s$) of TNF-α-free and TNF-α-containing (10 ng/mL) samples ($2.21 \pm 0.07\ \Omega\,cm^2$ vs. $2.20 \pm 0.08\ \Omega\,cm^2$). As a matter fact, the examined concentration was too low to influence the total amount of ions in the solution.

After the characterization of cell-free system, the laminin-containing DMEM was drained and replaced with the suspension of cardiomyocytes in DMEM. The freshly isolated cardiomyocytes were first incubated 1 h for the initial adhesion followed by washing off the residually suspending cells. According to our previous results (Qiu et al., 2008), cardiomyocytes adhered very fast to ECM within the first hour in cell culture and then slowly decreased the adhesion rate in the following hours. The 1-h initial incubation allowed most of viable cardiomyocytes to adhere to the ECM. The absolute cell–substrate distance was calculated through Lo's ECIS model (Lo and Ferrier, 1998). The best fit of ECIS (Fig. 3b) resulted in the absolute cell–substrate distance of 75.3 nm after 1-h initial incubation.

### 3.2. Stabilization of cardiomyocyte layer

The cardiomyocyte culture was needed to be incubated at least overnight to ensure the initial adhesion would not affect the result of the following chemical treatments. We monitored the stabilization of cardiomyocyte layer through impedance sensing since the non-adherent cardiomyocytes were washed away. The adhesion profile (Fig. 3c) showed that cardiomyocyte layer experienced a rapid adhesion process at the beginning in terms of the decreasing equivalent cell substrate distance. The fluctuation of curve indicated the cardiomyocyte layer was not so stable at this phase. The descent tendency ended at the distance of around 60 nm within 24 h of incubation, while the fluctuation was weakened at the same phase, suggesting the cardiomyocyte layer became necessarily stable for the following experiments. Besides the initial absolute cell–substrate distance calculated through ECIS, the absolute distances at $t = 12$ h and $t = 24$ h were also presented in Fig. 3c as

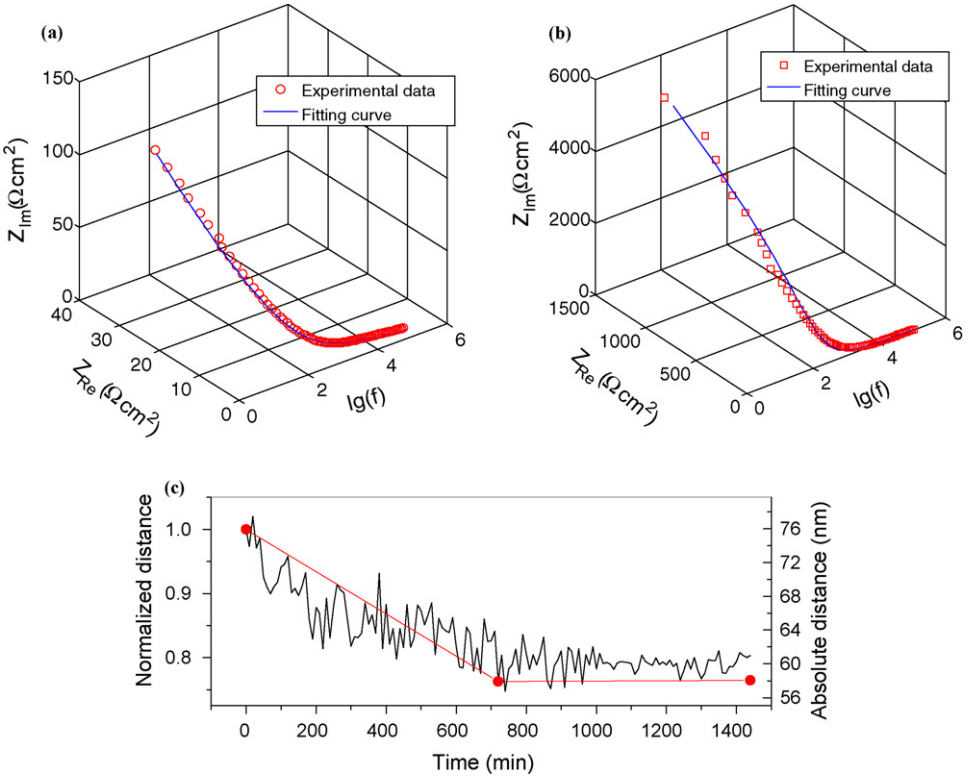


**Fig. 3.** (a) Characterization of cell-free impedance sensing system ($Z_n$) with CNLS curve fitting. (b) ECIS calibration of absolute cell–substrate distance based on Lo's model of cells (Lo and Ferrier, 1998). (c) The 24-h stabilization of cardiomyocyte layer. The time course of equivalent cell–substrate distance was plotted in solid line. The manual calibration with ECIS model was plotted in scattered dots which showed good agreement with the continuous time course.

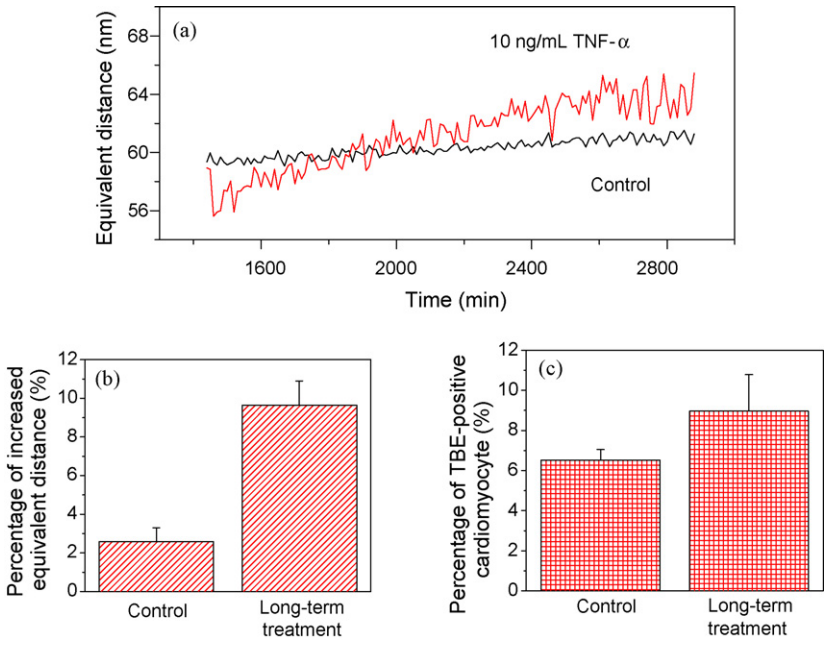


**Fig. 4.** (a) Representative cell-adhesion profiles of cardiomyocytes treated sustainedly by 10 ng/mL TNF-α. TNF-α-treated samples experienced the strengthening of cell adhesion at the beginning followed by the continuous weakening of cell adhesion. (b) After a 24-h incubation, the percentage of increased equivalent cell–substrate distance of the control and the long-term TNF-α-treated sample. Results shown were mean ± S.D. from three independent experiments. (c) TBE test results of the control and the 10 ng/mL TNF-α-treated cardiomyocytes. There was obvious difference between death percentages of the control and the TNF-α-treated sample ($P < 0.05$).

scattered data dots which showed their good agreement with the curve of equivalent cell–substrate distance.

### 3.3. The responses of cardiomyocytes treated continuously with TNF-α

After the stabilization for 24 h, cardiomyocytes were treated with TNF-α and monitored with our impedance-sensing technique. At the concentration level of 10 ng/mL TNF-α, the cardiomyocyte layer exhibited an adhesion profile beginning with a gentle cell attachment which was followed by sustained cell detachment in the later hours, as shown in Fig. 4a. The equivalent cell–substrate distance first decreased from its initial value of 58.9 nm to around 56 nm within 2 h, indicating the enhancement of cell adhesion. Afterwards, the cell–substrate distance began to increase. The ascent tendency of curves lasted till the end of 24-h monitoring, reaching a remarkable increment of 9.6 ± 1.3% nm (vs. 2.6 ± 0.7% of the control, Fig. 4b). Since cell detachment was one of the most important morphological phenomena of death processes, prompted cell death percentage was expected. The result of TBE test confirmed that cell death percentage was increased from by the continuous TNF-α treatment for 24 h (9.0 ± 1.8% vs. 6.5 ± 0.5% of the control, $P < 0.05$), as shown in Fig. 4c.

According to the published reports (Krown et al., 1996; Packer, 1995; Song et al., 2000; Takahashi et al., 2007; Zhu et al., 2006), TNF-α can trigger apoptotic signaling pathways which leads to cardiomyocyte detachment from ECM. Beside, the toxicity of TNF-α can also induce necrotic cell death in which the rapture of cell membrane leads to cell detachment. The real-time monitoring of cell adhesion provided a direct vision with quantitative and meaningful information that reflected the ongoing process of cardiomyocyte death. More importantly, since the activation of caspase family and cell membrane rapture both occur at the beginning of the corresponding death processes, it is possible to consider cell detachment as an early signal of cell death. The impedance-sensing technique for real-time monitoring cell adhesion enables the intervention of cell responses on the basis of inquired status quo. According to the results above, it took around 2 h to induce the cardiomyocyte detachment with TNF-α. It suggested the possibility to intervene in cardiomyocyte responses, i.e., to prevent them from cell death, by removing TNF-α before the critical moment of cell detachment.

### 3.4. The intervention of cardiomyocyte responses to TNF-α

The short-term treatment of TNF-α was carried out at the concentration of 10 ng/mL. After 2 h, TNF-α-containing medium was replaced with serum-free medium. The treated cardiomyocyte layer was continuously monitored since the beginning of TNF-α treatment. As shown in Fig. 5a, a rapid descent of cell–substrate distance occurred in the first 2 h of exposure, followed by a slow descent in the rest of 24-h monitoring. The cell–substrate distance curve of short-term treated cardiomyocytes showed a similar tendency with that of the long-term treated ones within the first 2 h, while the removal of TNF-α caused distinct tendencies afterwards. At the end of 24-h incubation, the short-term TNF-α treated sample exhibited a significant decrease in cell–substrate distance while that of the control sample was a slight increase (Fig. 5b). According to published reports (Eble et al., 2000; Huang et al., 2007), the cell adhesion plays an important role in the cell survival for the cell adhesion activates FAK signaling which will cancel out the apoptotic pathways. Once the cell adhesion was strengthened, the enhanced activation of FAK would further decrease the death percentage in cardiomyocytes. Furthermore, the removal of TNF-α also stopped the toxic condition of cardiomyocytes, so that the live cells would not go through necrotic death caused by TNF-α. Since the cell adhesion kept continuous enhancement in our experiments, it was possible that the death processes was interrupted by the removal of TNF-α. The suppressed cell apoptosis percentage and prompted cell viability of short-term treated cardiomyocyte samples were observed in TUNEL and TBE test, respectively. Fig. 5c showed the short-term treated cardiomyocytes exhibited a less TUNEL-positive percentage than the long-term sample (4.1 ± 1.4% vs. 11.3 ± 1.2%, $P < 0.01$) after a 24-h incubation, indicating the cardiomyocytes were prevented from apoptosis by the removal of TNF-α. As the

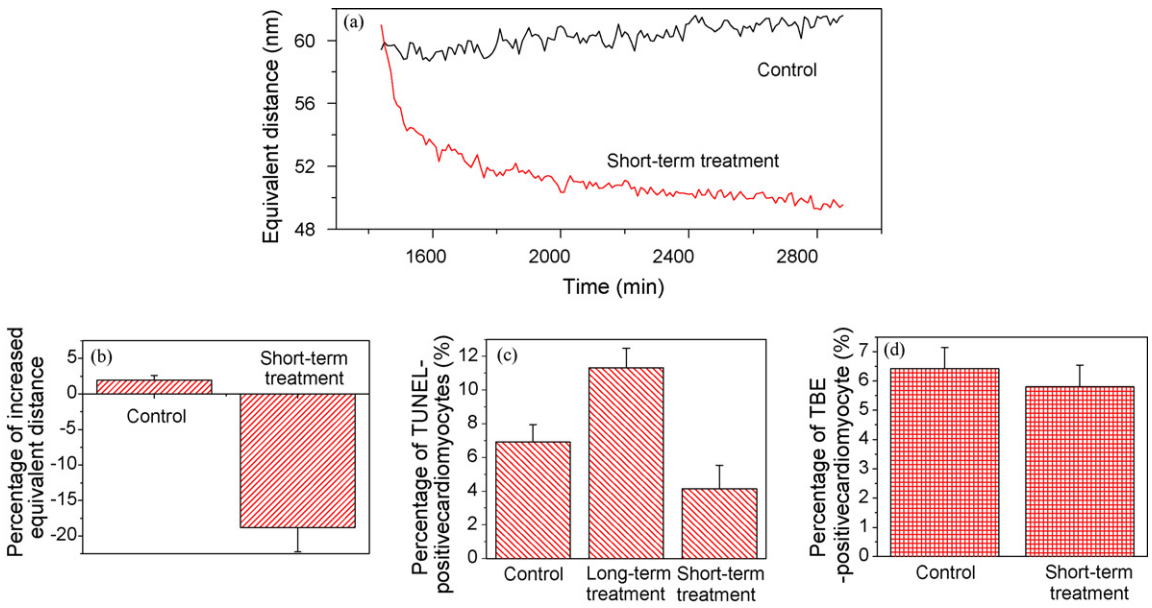


**Fig. 5.** (a) Representative cell-adhesion profiles in the short-term treated cardiomyocytes in 24 h. (b) After a 24-h incubation, the percentage of increased equivalent cell–substrate distance of the control and the short-term TNF-α-treated sample. Results shown were mean ± S.D. from three independent experiments. (c) TUNEL test results of the control, the long-term and the short-term treated samples of cardiomyocytes. The treated sample exhibit an obviously lower TUNEL-positive percentage than the control ($P < 0.01$). (d) TBE test results of the control and the short-term treated cardiomyocytes. There was no obvious difference between death percentages of the control and the short-term treated sample.

result of intervening in cell responses, the short-term treated cardiomyocytes also presented a low cell death percentage (5.8 ± 0.7%) in the TBE test (Fig. 5d) after a 24-h incubation. Comparing the death percentages with the control and the long-term treated cardiomyocytes, the short-term treatment with TNF-α tended to be promotional for the cell survival rather than the cell death. Moreover, the continuous enhancement of cell adhesion could be caused by cardiomyocyte hypertrophy induced by TNF-α. According to the published reports (Condorelli et al., 2002; Hiraoka et al., 2001; Yokoyama et al., 1997), TNF-α provokes cardiomyocyte hypertrophy in which the promotion of cell adhesion is one of the morphological evidences of cell–substrate interaction.

## 4. Conclusion

In this work, the intervention of cardiomyocyte responses and preventing of TNF-α-induced cell death were achieved through the impedance-sensing technique and the corresponding removal of chemical stimuli. The cell adhesion of cardiomyocytes was real-time monitored and used as the criterion of cell responses to the external stimuli. In our experiments, after the characterization of cardiomyocyte-based impedance-sensing system and the stabilization of cardiomyocyte layer for 24 h, TNF-α was applied to the stabilized cardiomyocytes to induce cell death in a sustained treatment while the monitoring of cell adhesion showed that it took around 2 h to provoke cell detachment. Since cell detachment was one of the morphological evidences at early phases of death mechanism, intervention could be applied before the critical moment of cell detachment to prevent cardiomyocytes from cell death. The removal of TNF-α from the cardiomyocyte culture was employed as the intervention in our experiments. Our results showed cell adhesion of cardiomyocytes was continuously strengthened with the removal of TNF-α. It was also demonstrated in TUNEL and TBE tests that the death percentage was lowered by the intervention of cardiomyocyte responses. In the field of cell biology, this novel sensing and intervention technique is promising to become a high throughput experimental approach which will benefits from its non-invasiveness and convenience.

## Acknowledgements

This work is in part supported by NSF CAREER Award (No. 0239163) and NSF NER Award (No. 0609147). The authors would like to thank Dr. Xu Wang, Dr. Bo Wang, Dr. Jianru Shi, Dr. Michael Bauer, and Jian Guan at Cardiac Muscle Research Laboratory, Brigham and Women's Hospital, Harvard Medical School for their technical advice.

## References

Aas, V., Torbla, S., Andersen, M.H., Jensen, J., Rustan, A.C., 2002. Annals of the New York Academy of Sciences 967, 506–515.
Arndt, S., Seebach, J., Psathaki, K., Galla, H.J., Wegener, J., 2004. Biosensors & Bioelectronics 19 (6), 583–594.
Bard, A.J., Faulkner, L.R., 2003. Electrochemical Methods: Fundamentals and Applications, second ed. John Wiley and Sons, Hoboken, NJ, USA.
Barsoukov, E., Macdonald, J.R., 2005. Impedance Spectroscopy, second ed. John Wiley & Sons, Inc, Hoboken, NJ, USA.
Condorelli, G., Morisco, C., Latronico, M.V., Claudio, P.P., Dent, P., Tsichlis, P., Condorelli, G., Frati, G., Drusco, A., Croce, C.M., Napoli, C., 2002. FASEB J 16 (13), 1732–1737.
Cook, S.A., Poole-Wilson, P.A., 1999. European Heart Journal 20 (22), 1619–1629.
Earley, S., Plopper, G.E., 2006. Biochemical and Biophysical Research Communications 350 (2), 405–412.
Eble, D.M., Strait, J.B., Govindarajan, G., Lou, J., Byron, K.L., Samarel, A.M., 2000. American Journal of Physiology: Heart and Circulatory Physiology 278 (5), H1695–1707.
Giaever, I., Keese, C.R., 1984. Proceedings of the National Academy of Sciences of United States of America 81 (12), 3761–3764.
Giaever, I., Keese, C.R., 1991. Proceedings of the National Academy of Sciences of United States of America 88 (17), 7896–7900.
Giaever, I., Keese, C.R., 1993. Nature 366 (6455), 591–592.
Haunstetter, A., Izumo, S., 1998. Circulation Research 82, 1111–1129.
Hengartner, M.O., 2000. Nature 407 (6805), 770–776.
Hiraoka, E., Kawashima, S., Takahashi, T., Rikitake, Y., Kitamura, T., Ogawa, W., Yokoyama, M., 2001. American Journal of Physiology: Heart and Circulatory Physiology 280 (4), H1861–1868.
Huang, D., Khoe, M., Befekadu, M., Chung, S., Takata, Y., Ilic, D., Bryer-Ash, M., 2007. American Journal of Physiology 292 (4), C1339–1352.
Kowolenko, M., Keese, C.R., Lawrence, D.A., Giaever, I., 1990. Journal of Immunological Methods 127 (1), 71–77.
Krown, K.A., Page, M.T., Nguyen, C., Zechner, D., Gutierrez, V., Comstock, K.L., Glembotski, C.C., Quintana, P.J., Sabbadini, R.A., 1996. The Journal of Clinical Investigation 98 (12), 2854–2865.
Lim, C.C., Helmes, M.H., Sawyer, D.B., Jain, M., Liao, R., 2001. American Journal of Physiology: Heart and Circulatory Physiology 281 (2), H969–974.

Lo, C.M., Ferrier, J., 1998. Physics Review E 57 (6), 6982–6987.
Lo, C.M., Keese, C.R., Giaever, I., 1995. Biophysical Journal 69 (6), 2800–2807.
Luong, J.H.T., Habibi-Rezaei, M., Meghrous, J., Xiao, C., Male, K.B., Kamen, A., 2001. Analytical Chemistry 73 (8), 1844–1848.
Packer, M., 1995. Circulation 92 (6), 1379–1382.
Qiu, Y., Liao, R., Zhang, X., 2008. Analytical Chemistry 80 (4), 990–996.
Qiu, Y., Liao, R., Zhang, X., 2009. Biophysical Journal 96 (5), 1985–1991.
Song, W., Lu, X., Feng, Q., 2000. Cardiovascular Research 45 (3), 595–602.
Takahashi, R., Sonoda, Y., Ichikawa, D., Yoshida, N., Eriko, A.Y., Tadashi, K., 2007. Biochimica et Biophysica Acta 1770 (4), 518–526.
Tiruppathi, C., Malik, A.B., Del Vecchio, P.J., Keese, C.R., Giaever, I., 1992. Proceedings of the National Academy of Sciences of United States of America 89 (17), 7919–7923.
Tlili, C., Reybier, K., Geloen, A., Ponsonnet, L., Martelet, C., Ouada, H.B., Lagarde, M., Jaffrezic-Renault, N., 2003. Analytical Chemistry 75 (14), 3340–3344.
Xiao, C., Lachance, B., Sunahara, G., Luong, J.H., 2002. Analytical Chemistry 74 (6), 1333–1339.
Yang, M., Lim, C.C., Liao, R., Zhang, X., 2007. Biosensors & Bioelectronics 22, 1688–1693.
Yang, M., Zhang, X., 2007. Sensors and Actuators A Physical 136 (2), 504–509.
Yokoyama, T., Nakano, M., Bednarczyk, J.L., McIntyre, B.W., Entman, M., Mann, D.L., 1997. Circulation 95 (5), 1247–1252.
Zhu, J., Liu, M., Kennedy, R.H., Liu, S.J., 2006. Cytokine 34 (1-2), 96–105.